THE JOURNAL OF PHYSICAL CHEMISTRY B
A JOURNAL OF THE AMERICAN CHEMICAL SOCIETY

pubs.acs.org/JPCB

Article

Structure and Orientation of the SARS-Coronavirus-2 Spike Protein at Air−Water Interfaces

Mikkel Bregnhøj, Steven J. Roeters,* Adam S. Chatterley, Fani Madzharova, Rolf Mertig, Jan Skov Pedersen, and Tobias Weidner*

Cite This: https://doi.org/10.1021/acs.jpcb.2c01272

Read Online

ACCESS | Metrics & More | Article Recommendations | Supporting Information

ABSTRACT: The SARS coronavirus 2 (SARS-CoV-2) spike protein is located at the outermost perimeter of the viral envelope and is the first component of the virus to make contact with surrounding interfaces. The stability of the spike protein when in contact with surfaces plays a deciding role for infection pathways and for the viability of the virus after surface contact. While cryo-EM structures of the spike protein have been solved with high resolution and structural studies in solution have provided information about the secondary and tertiary structures, only little is known about the folding when adsorbed to surfaces. We here report on the secondary structure and orientation of the S1 segment of the spike protein, which is often used as a model protein for in vitro studies of SARS-CoV-2, at the air−water interface using surface-sensitive vibrational sum-frequency generation (SFG) spectroscopy. The air−water interface plays an important role for SARS-CoV-2 when suspended in aerosol droplets, and it serves as a model system for hydrophobic surfaces in general. The SFG experiments show that the S1 segment of the spike protein remains folded at the air−water interface and predominantly binds in its monomeric state, while the combination of small-angle X-ray scattering and two-dimensional infrared spectroscopy measurements indicate that it forms hexamers with the same secondary structure in aqueous solution.

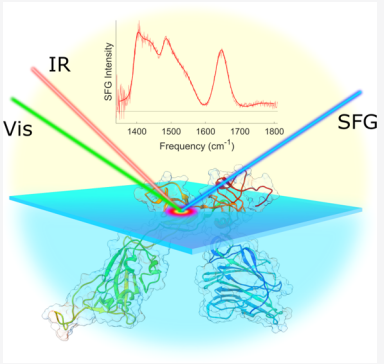

1. INTRODUCTION

The spike protein of SARS coronavirus 2 (SARS-CoV-2) is the key molecule for viral entry into human cells as it is the first contact point with host cells and therefore crucial for viral viability and reproduction. As such, it is a prime target for the immune response, antigen testing, and vaccines. The structure of the spike protein has been studied intensively, and X-ray crystal structures, cryo-EM, as well as solution-state studies have provided detailed information about the secondary and tertiary structure.[1−5] However, surface contacts can change the protein structure severely and, to the best of our knowledge, only theoretical studies have been reported about the folding of the spike protein when in contact with surfaces.[6,7]

We here report experimental evidence on the structure and orientation of the spike protein adsorbed to the air−water interface (AWI). The AWI is a hydrophobic interface, which is potentially a very disruptive surface and known to alter protein structure in many cases.[8−10] The AWI plays an important role for SARS-CoV-2 when airborne within aerosol droplets, suspended in test tubes, or bound to the surfaces within the respiratory tract. Besides this direct role, the AWI is also a good model system for hydrophobic surfaces in general and can therefore provide a first approximation of how the spike protein will respond to natural and technical hydrophobic surfaces such as plant surfaces, test tubes, coatings, textiles, and skin.

To determine the structure of the SARS-CoV-2 spike protein at the AWI and in bulk aqueous solution, we combine vibrational sum frequency generation (SFG) spectroscopy with two-dimensional infrared (2D-IR) spectroscopy and small-angle X-ray scattering (SAXS). SFG spectroscopy in the amide I and amide II regions can determine how proteins fold and orient specifically at interfaces.[11−13] Mixing broadband infrared laser pulses with narrowband visible laser pulses at the interface generates sum frequency photons, which report on vibrational modes at the interface.[14] On the other hand, 2D-IR and SAXS data provide information about the secondary structure and aggregation state of the protein in solution.[15,16]

Together, we find that the SARS-CoV-2 spike protein remains intact when binding to the AWI and predominantly binds in its monomeric state.

2. METHODS

Further details about experiments and data analysis can be found in the Supporting Information.

Received: February 22, 2022
Revised: April 6, 2022

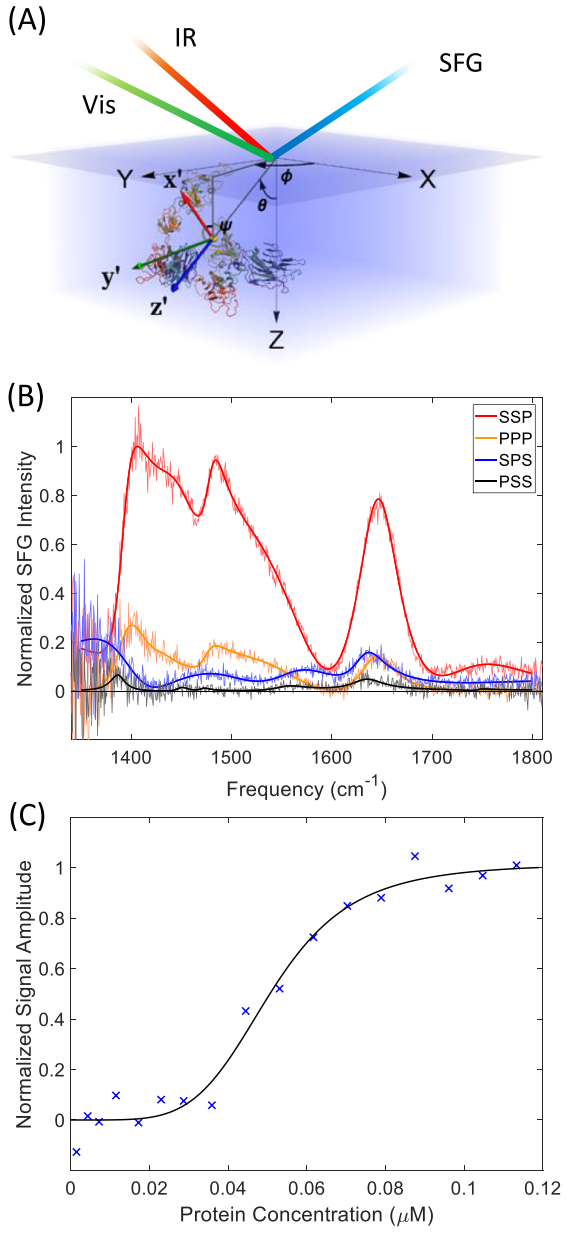

Figure 1. Experimental characterization of the spike protein at the air−water interface with SFG spectroscopy. (A) Schematic overview of the experimental setup with incoming and outgoing laser beams. Also shown are the relevant angles and coordinate systems of the protein relative to the interface. (B) Normalized SFG spectra of the spike protein injected into a trough with phosphate-buffered D_2O to a concentration of 0.3 μM. The spectra are recorded in ssp (red), ppp (orange), sps (blue), and pss (black) polarization combinations, respectively. For further clarity, the spectra have been plotted individually in the Supporting Information. (C) Normalized SFG signal amplitude of the amide I band at 1647 cm^{-1}, plotted as a function of the added spike protein concentration in the bulk. The black solid line is a fit to a modified Langmuir/Hill equation for protein surface adsorption (see Supporting Information for details).

2.1. Sample Preparation. The S1 segment of the SARS-CoV-2 spike protein (residues Gln14-Arg685) was purchased from GenScript Biotech (purity > 85%), and the sequence and purity were checked by mass spectrometry. The samples were kept at −80 °C until use. Upon thawing, the samples were buffer-exchanged into D_2O-based phosphate (PBS) buffer and diluted to the desired concentration for a given experiment.

2.2. SFG Spectroscopy. The SFG experiments were conducted on a home-built setup described in detail elsewhere.[17] Briefly, we used an amplified Ti:Sapphire laser system (Astrella, Coherent) to generate broadband mid-infrared light (TOPAS Prime, Light Conversion) and narrowband visible light through an etalon (fwhm ≈ 16 cm^{-1}), which were overlapped on the sample in time and space. The resultant SFG light was directed onto a spectrograph and camera (Shamrock/Newton, Andor) for spectral acquisition. The spectra were background subtracted and normalized to the spectrum from a clean gold sample.

2.3. Small-Angle X-ray Scattering. SAXS data were recorded at the HyperSAXS facility in Aarhus, Denmark.[18] The data were calibrated to an absolute scale and displayed as a function of the modulus of the scattering vector, q. The forward scattering data yield a mass of about 390 kDa corresponding to six spike proteins per scatterer. The SAXS data were modeled by rigid-body refinement with 10 independent runs per input structure using home-written software.[19]

2.4. Two-Dimensional Infrared Spectroscopy. Transmission two-dimensional infrared (2D-IR) spectra were recorded using a commercial instrument set to operate in the amide I region (2DQuickIR, PhaseTech Spectroscopy), as described previously.[20] Briefly, a time delayed collinear pair of femtosecond infrared pump pulses were produced using a pulse shaper, and the transmission spectrum of the pumped sample was measured using a third, non-collinear, infrared pulse that was dispersed on a grating spectrometer and measured using a high repetition rate MCT detector (Jackhammer, PhaseTech Spectroscopy). Fourier transformation with respect to the delay between the pump pulses produced the 2D-IR spectra shown.

2.5. Spectral Calculations. The SFG spectra are calculated based on the formalism reported previously.[21] Briefly, we construct a one-exiton amide I Hamiltonian based on the atomic positions of the backbone amide groups. The couplings between the nearest neighbors (dominated by through-bond interactions) are determined using a parameterized map of the coupling as a function of the dihedral angle derived from a ab initio calculation of "glycine dipeptide" (Ac-Gly-NHCH3) using the 6-31G+(d) basis set and B3LYP-functional,[22] while all other couplings (dominated by through-space interactions) are calculated using the transition-dipole coupling model (TDCM).[23] We diagonalize the Hamiltonian to obtain the eigenvalues and eigenvectors of the eigenmodes, from which the IR and Raman responses, and their outer product, the SFG hyperpolarizability tensor, are determined.

For the 2D-IR spectral calculations, the corresponding 2-exciton Hamiltonian is constructed using the formalism described by Hamm and Zanni,[24] which leads to such large matrices for the S1 spike protein that the diagonalization is computationally very challenging. Therefore, we have cut up the 670 residue monomers into 3 segments of almost equal length and averaged the 2D-IR response of the 18 segments that are thus created for the hexamer structure. Because the couplings decrease with the inter-amide-group distance to the third power, this should only lead to a minimal loss of the couplings that shape the 2D-IR amide I spectrum.

3. RESULTS

3.1. Surface Studies. For the SFG experiments, we inject the S1 segment of the spike protein (Val16-Arg685),

https://doi.org/10.1021/acs.jpcb.2c01272
J. Phys. Chem. B XXXX, XXX, XXX−XXX

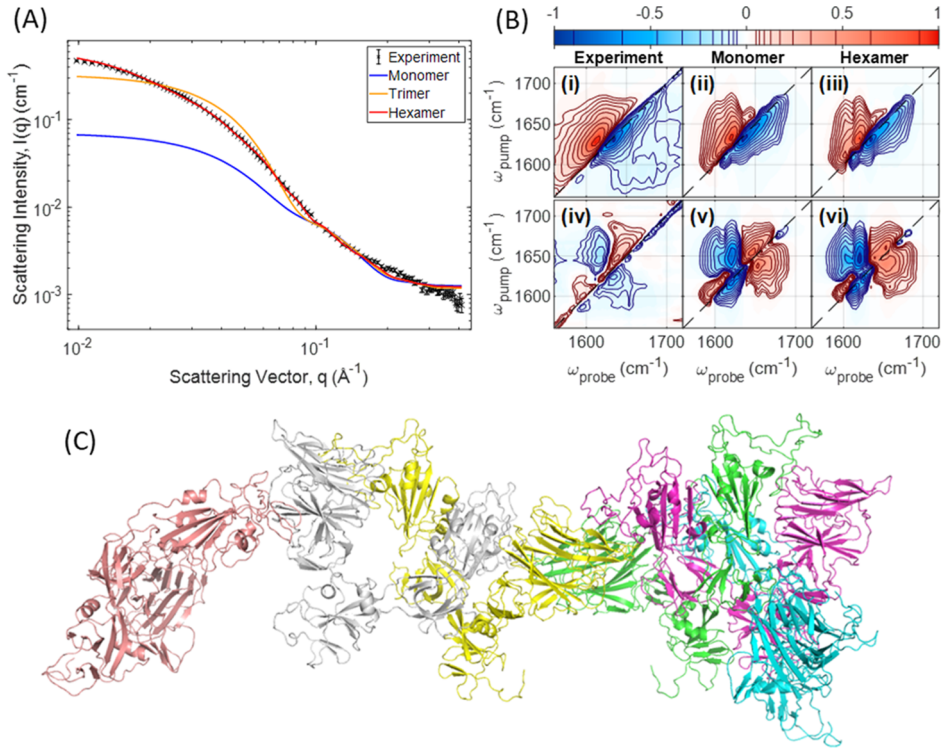

Figure 2. Structural characterization of the spike protein in bulk solution with SAXS and 2D-IR spectroscopy. (A) Experimental SAXS data (black crosses) superimposed with the model fit from the hexamer structure (red line). Representative model fits for the monomer (blue) and trimer (orange) structures are also shown for comparison. (B) Measured 2D-IR spectrum of the (i) spike protein with pump and probe beams polarized parallel to each other, alongside the calculated spectra for the protein in its monomeric (ii) or hexameric (iii) form and the corresponding difference between the normalized parallel and perpendicular polarized 2D-IR spectra (iv–vi). In these parallel–perpendicular difference spectra, the diagonal features are removed, which enhances the sensitivity to the cross-peaks that directly show the coupling between vibrational modes. Note that, to enhance weak features, the contours are not uniformly spaced—the lines within the color bar show the contour positions. (C) Illustration of one of the hexameric spike structures, which gives the best match to the experimental SAXS data. Each monomer unit within the structure has its own distinct color. Please note that this structure is not unique in modeling the SAXS data, but just one of the SAXS-derived hexamer structures that we include in our calculations.

responsible for the initial interaction with binding partners and surfaces, into the subphase of a trough and overlap the laser beams at the aqueous surface. An illustration of the experimental geometry is shown in Figure 1A. The frequencies of the infrared beam were chosen to cover the amide I and amide II spectral regions (1350–1800 cm^{-1}). We prepared our samples using buffer based on D_2O instead of H_2O to avoid interference from water bending modes in this spectral region. This also leads to deuteration of the N atoms in the amide groups, which modifies the amide I and amide II modes to their deuterated equivalents (denoted amide I′ and amide II′).

SFG spectra for different polarization combinations of the incoming and outgoing laser beams are displayed in Figure 1B. Given the chosen beam angles, the most intense spectra are observed in the ssp combination (s-polarized SFG, s-polarized visible, and p-polarized IR). The broad peak around 1650 cm^{-1} can be assigned to the amide I′ band. The width of the peak reflects the structural variation present within this relatively large protein. The weak mode near 1750 cm^{-1} can be assigned to sidechain C═O modes. There are several broad resonances below 1600 cm^{-1}. The shoulder near 1500 cm^{-1} is likely assigned to protonated C═O groups, and the signal near 1450 cm^{-1} is likely related to the side chain C–H bending modes. The feature near 1460 cm^{-1} is assigned to the amide II′ backbone mode. Spectra recorded in other polarization combinations show most of the same modes with different intensities (see Figure 1B and the Supporting Information).

The selection rules of SFG dictate that only ordered species at an interface are visible in the spectra. A disordered structure or signal from proteins in solution near the surface cancels in the far-field (doi.org/10.1116/6.0001401). Therefore, the presence of backbone and sidechain modes in the spectra imply that the spike protein forms a relatively well-ordered layer at the air–water interface. In order to investigate the propensity of the spike protein to bind to the AWI, we recorded SFG spectra as a function of protein concentration, where the protein coverage of the surface was tracked using the intensity of the amide I′ band at 1647 cm^{-1} (Figure 1C). This analysis show that the spike protein binds relatively strongly to the surface with an apparent binding constant of $(2.3 \pm 0.3) \times 10^6$ $\mu M^{-4.9}$. The Hill coefficient of 4.9 extracted from the binding isotherm indicates cooperative binding to the air–water interface, which suggests attractive interactions between spike proteins at the water surface (see Supporting Information for details).

3.2. Structural Analysis. Since SFG is a coherent method and spectra from structurally diverse proteins are the result of complex interferences between SFG photons, the data cannot be reliably interpreted by spectral inspection or fitting alone. To compare the cryo-EM structure of the spike protein with SFG data directly, and thereby determine the folding state and

https://doi.org/10.1021/acs.jpcb.2c01272
J. Phys. Chem. B XXXX, XXX, XXX–XXX

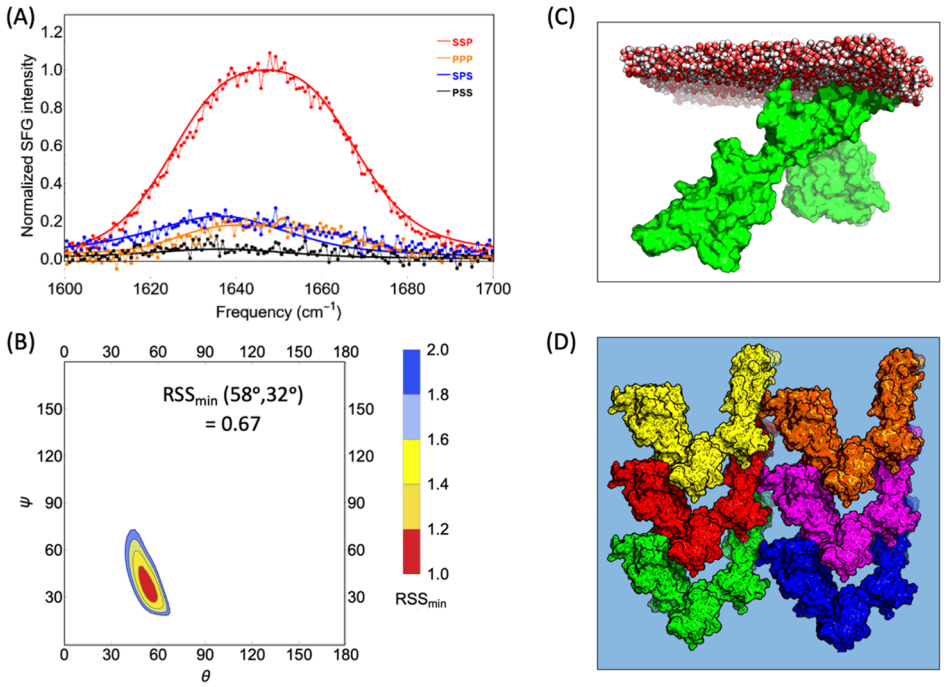

Figure 3. Calculated SFG spectra for the best-matching monomeric open-form protein structure. (A) Comparison of the best matching calculated SFG spectra in the amide I region to experimental data for four different polarization combinations. Spectra for all other structures are shown in the Supporting Information. (B) Residual sum-squares error (RSS) plot showing the optimal tilt (θ) and twist (Ψ) angles of the monomer protein with respect to the surface, which was used to produce the spectra shown in panel (A). (C) Illustration of the spike protein in the best-matching orientation at the air−water interface. (D) Top-view of a lateral arrangement of spike proteins within the monolayer, which is in agreement with the experimental data. In this model, the spike monomers are interacting laterally through β-sheet structures, forming a densely packed layer at the water surface.

orientation of the spike protein at the surface, we calculate the theoretical amide I SFG response and compare the calculated spectra with the experimental data. The calculations are based on the cryo-EM derived SARS-CoV-2 spike structures[3] in the open and closed states (PDB entries 6VXX and 6VYB, respectively), which have been structurally completed using the C−I-TASSER algorithm.[25]

For the calculations, we have to take the aggregation state of the spike protein into account. While the protein is known to form homo-trimers at the viral surface,[4,26,27] the oligomeric state of our recombinantly expressed protein in solution is not known. To investigate this, we use SAXS and 2D-IR spectroscopy, as shown in Figure 2. SAXS profiles for the spike protein in solution indicate that, when testing a variety of cluster sizes and starting structures, a hexameric cluster is dominating the solution-state ensemble (Figure 2A,C). Furthermore, when we compare the experimental 2D-IR spectrum with the calculated 2D-IR spectrum for the SAXS-derived hexamer structures (Figure 2B), we find a match that is consistent with a globular protein structure that contains both α-helical and β-sheet secondary structure elements.[16] This makes it unlikely that the formation of the hexameric oligomers causes a large change in the secondary structure, for example, to amyloid aggregates, which have distinct sharp peaks in the 2D-IR spectrum,[28] very different from the ones observed here for the spike protein.

However, since surfaces are known to potentially disrupt protein clusters,[8] and since the concentration of protein at the interface is unknown, we cannot immediately rule out any of these aggregation states for the protein when bound to the surface. Therefore, we include the monomeric state, a dimer state, and the native trimeric state along with an ensemble of SAXS-derived hexameric structures as potential starting binding poses in our SFG calculations. Furthermore, we also take into account the fact that the protein can reside at the interface in either an open or a closed form. The former is characteristic of the spike protein when situated at the viral envelope, while the latter is observed for proteins interacting with its target receptor ACE2.

Consequently, we run our SFG spectral calculations for a map of all possible different tilt and twist angles for monomer, dimer, and trimer structures, in both open and closed forms, and 30 different structural models based on the SAXS data. We then rank the structures by the resemblance of the experimental and the calculated SFG spectra for each structural model. A summary of all structural models and the associated calculated spectra can be found in the Supporting Information. Overall, the monomeric structure in the open form shows the best match with the experimental data, as shown in Figure 3A. The calculations converge on this result irrespective of our starting choice of the spectral parameters (see Supporting Information). We find the best match for the open form protein, as is expected, given that there are no receptors capable of binding to and closing the protein present in our system. The calculations match the experimental data very well for all the achiral polarization combinations when the monomeric protein adopt a slightly tilted binding geometry of about 58° with respect to the surface (Figure 3B). The residual-sum-of-squares (RRS) error value in this conformation is less than 0.67, which is much smaller than the minimal RSS value obtained for the other structures (Figure S4). A

https://doi.org/10.1021/acs.jpcb.2c01272
J. Phys. Chem. B XXXX, XXX, XXX−XXX

schematic of the binding geometry of the monomer at the air–water interface is shown in Figure 3C.

The second-best match (RSS = 1.3) was achieved for the trimer model in a somewhat more inclined binding orientation of 65° (see Supporting Information). The dimer model did not match the experimental data well, with a deviation of more than RSS = 2.6. The SAXS structures, which describes the solution-state clusters well, did not match the experimental SFG data in any orientation (RSS higher than 2.4). Ostensibly, the hexameric spike protein clusters in solution are not stabilized at the AWI but break down into smaller units and rearrange significantly when interacting with the surface.

4. DISCUSSION

4.1. Spike Protein Interaction with the Air–Water Interface. The spike protein layer at the AWI is essentially a large assembly that promotes lateral protein interactions in combination with the surface interaction. Likely, the delicate balance of forces, which steers the proteins into different types of clusters, is shifted toward a more aligned assembly of monomer spike proteins when bound to the surface. The binding geometry will depend on several factors, including the interaction with the AWI, interaction between monomers, and solvation energy. An aligned, tilted binding geometry, inferred here for the spike protein, is often observed for interfacial structures and proteins, where it is important to maximize lateral as well as surface interactions simultaneously.[29−32]

Strong lateral interactions between spike proteins within the surface layer are also manifested in the appearance of the intense amide II′ band (Figure 1B). This band is SFG inactive for most proteins and is usually only observed when vibrational modes are highly delocalized across the protein structure, for example, within large aggregates such as amyloid fibers.[33−35] In this context, our data suggest that the spike proteins are strongly coupled to each other when forming a densely packed protein layer the air–water interface, while still retaining their monomeric structure within this layer. A packing geometry in agreement with these results is shown in a top view in Figure 3D. In the displayed binding structure, the packing density of the monomers is high and lateral interactions through β-strand sites is maximized. We note that, while the shown assembly is in agreement with the structural data, there is no direct evidence for the model at this point.

5. CONCLUSIONS

Together, the data show that the SARS-CoV-2 spike protein is strongly attracted to the air–water interface. The protein binds to the AWI as monomers and assumes a slightly tilted orientation. Since the AWI is a model for hydrophobic surfaces in general, this implies that the spike protein will likely bind to other hydrophobic surfaces as well. Unlike many other globular proteins, it can be expected that the protein will stay intact during contact with hydrophobic surfaces such as polymers, plant surfaces, skin, aerosol particles, and test tubes as well as to gas bubbles in non-degassed buffers.

■ ASSOCIATED CONTENT

Supporting Information

The Supporting Information is available free of charge at https://pubs.acs.org/doi/10.1021/acs.jpcb.2c01272.

Further details about the experimental setup, SFG fitting parameters, binding constant of the spike protein, SAXS and 2D-IR spectra, and all calculated spectra (PDF)

■ AUTHOR INFORMATION

Corresponding Authors

Steven J. Roeters − *Department of Chemistry, Aarhus University, 8000 Aarhus C, Denmark;* orcid.org/0000-0003-3238-2181; Email: s.j.roeters@chem.au.dk

Tobias Weidner − *Department of Chemistry, Aarhus University, 8000 Aarhus C, Denmark;* orcid.org/0000-0002-7083-7004; Email: weidner@chem.au.dk

Authors

Mikkel Bregnhøj − *Department of Chemistry, Aarhus University, 8000 Aarhus C, Denmark;* orcid.org/0000-0001-5748-6783

Adam S. Chatterley − *Department of Chemistry, Aarhus University, 8000 Aarhus C, Denmark;* orcid.org/0000-0003-3847-5936

Fani Madzharova − *Department of Chemistry, Aarhus University, 8000 Aarhus C, Denmark;* orcid.org/0000-0002-6748-1254

Rolf Mertig − *Department of Chemistry, Aarhus University, 8000 Aarhus C, Denmark*

Jan Skov Pedersen − *Department of Chemistry, Aarhus University, 8000 Aarhus C, Denmark;* orcid.org/0000-0002-7768-0206

Complete contact information is available at: https://pubs.acs.org/10.1021/acs.jpcb.2c01272

Author Contributions

M.B., S.J.R., and T.W. conceptualized the research. M.B. performed and analyzed the SFG experiments. A.S.C. and F.M. performed and analyzed the 2D-IR experiments. J.S.P. performed and analyzed the SAXS experiments. S.J.R. and R.M. performed and designed the spectral calculations. M.B., S.J.R., and T.W. wrote the communication with input from all co-authors.

Notes

The authors declare no competing financial interest.

Data Availability: All spectroscopic data are available from the authors upon reasonable request. Code Availability: The code used to calculate SFG and 2D-IR spectra is available from the authors upon reasonable request.

■ ACKNOWLEDGMENTS

This article is part of a project that has received funding from the European Research Council (ERC) under the European Union's Horizon 2020 research and innovation program (Grant agreement no. 819039 F-BioIce). T.W. acknowledges support by the Novo Nordisk Foundation (Facility Grant NanoScat, no. NNF18OC0032628).

■ REFERENCES

(1) Lan, J.; Ge, J.; Yu, J.; Shan, S.; Zhou, H.; Fan, S.; Zhang, Q.; Shi, X.; Wang, Q.; Zhang, L.; Wang, X. Structure of the SARS-CoV-2 Spike Receptor-Binding Domain Bound to the ACE2 Receptor. *Nature* **2020**, *581*, 215−220.

(2) Daly, J. L.; Simonetti, B.; Klein, K.; Chen, K.-E.; Williamson, M. K.; Antón-Plágaro, C.; Shoemark, D. K.; Simón-Gracia, L.; Bauer, M.; Hollandi, R.; Greber, U. F.; Horvath, P.; Sessions, R. B.; Helenius, A.; Hiscox, J. A.; Teesalu, T.; Matthews, D. A.; Davidson, A. D.; Collins,

B. M.; Cullen, P. J.; Yamauchi, Y. Neuropilin-1 Is a Host Factor for SARS-CoV-2 Infection. *Science* **2020**, *370*, 861−865.
(3) Walls, A. C.; Park, Y.-J.; Tortorici, M. A.; Wall, A.; McGuire, A. T.; Veesler, D. Structure, Function, and Antigenicity of the SARS-CoV-2 Spike Glycoprotein. *Cell* **2020**, *181*, 281−292.e6.
(4) Turoňová, B.; Sikora, M.; Schürmann, C.; Hagen, W. J. H.; Welsch, S.; Blanc, F. E. C.; von Bülow, S.; Gecht, M.; Bagola, K.; Hörner, C.; van Zandbergen, G.; Landry, J.; de Azevedo, N. T. D.; Mosalaganti, S.; Schwarz, A.; Covino, R.; Mühlebach, M. D.; Hummer, G.; Krijnse Locker, J.; Beck, M. In Situ Structural Analysis of SARS-CoV-2 Spike Reveals Flexibility Mediated by Three Hinges. *Science* **2020**, *370*, 203−208.
(5) Cai, Y.; Zhang, J.; Xiao, T.; Peng, H.; Sterling, S. M.; Walsh, R. M.; Rawson, S.; Rits-Volloch, S.; Chen, B. Distinct Conformational States of SARS-CoV-2 Spike Protein. *Science* **2020**, *369*, 1586−1592.
(6) Malaspina, D. C.; Faraudo, J. Computer Simulations of the Interaction between SARS-CoV-2 Spike Glycoprotein and Different Surfaces. *Biointerphases* **2020**, *15*, 051008.
(7) Benková, Z.; Cordeiro, M. N. D. S. Structural Behavior of Monomer of SARS-CoV-2 Spike Protein during Initial Stage of Adsorption on Graphene. *Mater. Today Chem.* **2021**, *22*, 100572.
(8) D'Imprima, E.; Floris, D.; Joppe, M.; Sánchez, R.; Grininger, M.; Kühlbrandt, W. Protein Denaturation at the Air-Water Interface and How to Prevent It. *eLife* **2019**, *8*, No. e42747.
(9) Schach, D.; Globisch, C.; Roeters, S. J.; Woutersen, S.; Fuchs, A.; Weiss, C. K.; Backus, E. H. G.; Landfester, K.; Bonn, M.; Peter, C.; Weidner, T. Sticky water surfaces: Helix-coil transitions suppressed in a cell-penetrating peptide at the air-water interface. *J. Chem. Phys.* **2014**, *141*, 22D517.
(10) Kim, J.; Somorjai, G. A. Molecular Packing of Lysozyme, Fibrinogen, and Bovine Serum Albumin on Hydrophilic and Hydrophobic Surfaces Studied by Infrared−Visible Sum Frequency Generation and Fluorescence Microscopy. *J. Am. Chem. Soc.* **2003**, *125*, 3150−3158.
(11) Hosseinpour, S.; Roeters, S. J.; Bonn, M.; Peukert, W.; Woutersen, S.; Weidner, T. Structure and Dynamics of Interfacial Peptides and Proteins from Vibrational Sum-Frequency Generation Spectroscopy. *Chem. Rev.* **2020**, *120*, 3420−3465.
(12) Weidner, T.; Castner, D. G. Developments and Ongoing Challenges for Analysis of Surface-Bound Proteins. *Annu. Rev. Anal. Chem.* **2021**, *14*, 389−412.
(13) Fu, L.; Wang, Z.; Yan, E. C. Y. Chiral Vibrational Structures of Proteins at Interfaces Probed by Sum Frequency Generation Spectroscopy. *Int. J. Mol. Sci.* **2011**, *12*, 9404−9425.
(14) Shen, Y. R. *Fundamentals of Sum-Frequency Spectroscopy*; Cambridge University Press, 2016.
(15) Larsen, A. H.; Pedersen, J. S.; Arleth, L. Assessment of Structure Factors for Analysis of Small-Angle Scattering Data from Desired or Undesired Aggregates. *J. Appl. Crystallogr.* **2020**, *53*, 991−1005.
(16) Ganim, Z.; Chung, H. S.; Smith, A. W.; DeFlores, L. P.; Jones, K. C.; Tokmakoff, A. Amide I Two-Dimensional Infrared Spectroscopy of Proteins. *Acc. Chem. Res.* **2008**, *41*, 432−441.
(17) Golbek, T. W.; Schmüser, L.; Rasmussen, M. H.; Poulsen, T. B.; Weidner, T. Lasalocid Acid Antibiotic at a Membrane Surface Probed by Sum Frequency Generation Spectroscopy. *Langmuir* **2020**, *36*, 3184−3192.
(18) Lyngsø, J.; Pedersen, J. S. A High-Flux Automated Laboratory Small-Angle X-Ray Scattering Instrument Optimized for Solution Scattering. *J. Appl. Crystallogr.* **2021**, *54*, 295−305.
(19) Harwood, S. L.; Lyngsø, J.; Zarantonello, A.; Kjøge, K.; Nielsen, P. K.; Andersen, G. R.; Pedersen, J. S.; Enghild, J. J. Structural Investigations of Human A2M Identify a Hollow Native Conformation That Underlies Its Distinctive Protease-Trapping Mechanism. *Mol. Cell. Proteomics* **2021**, *20*, 100090.
(20) Madzharova, F.; Bregnhøj, M.; Chatterley, A. S.; Løvschall, K. B.; Drace, T.; Andersen Dreyer, L. S.; Boesen, T.; Weidner, T. Electrostatics Trigger Interfacial Self-Assembly of Bacterial Ice Nucleators. *Biomacromolecules* **2022**, *23*, 505.
(21) Roeters, S. J.; van Dijk, C. N.; Torres-Knoop, A.; Backus, E. H. G.; Campen, R. K.; Bonn, M.; Woutersen, S. Determining In Situ Protein Conformation and Orientation from the Amide-I Sum-Frequency Generation Spectrum: Theory and Experiment. *J. Phys. Chem. A* **2013**, *117*, 6311−6322.
(22) Gorbunov, R. D.; Kosov, D. S.; Stock, G. Ab Initio-Based Exciton Model of Amide I Vibrations in Peptides: Definition, Conformational Dependence, and Transferability. *J. Chem. Phys.* **2005**, *122*, 224904.
(23) Krimm, S.; Bandekar, J. Vibrational Spectroscopy and Conformation of Peptides, Polypeptides, and Proteins. *Advances in Protein Chemistry*; Anfinsen, C. B., Edsall, J. T., Richards, F. M., Eds.; Academic Press, 1986; Vol. *38*, pp 181−364.
(24) Hamm, P.; Zanni, M. *Concepts and Methods of 2D Infrared Spectroscopy*; Cambridge University Press, 2011.
(25) Zheng, W.; Zhang, C.; Li, Y.; Pearce, R.; Bell, E. W.; Zhang, Y. Folding Non-Homologous Proteins by Coupling Deep-Learning Contact Maps with I-TASSER Assembly Simulations. *Cells Rep. Methods* **2021**, *1*, 100014.
(26) Hoffmann, M.; Kleine-Weber, H.; Schroeder, S.; Krüger, N.; Herrler, T.; Erichsen, S.; Schiergens, T. S.; Herrler, G.; Wu, N.-H.; Nitsche, A.; Müller, M. A.; Drosten, C.; Pöhlmann, S. SARS-CoV-2 Cell Entry Depends on ACE2 and TMPRSS2 and Is Blocked by a Clinically Proven Protease Inhibitor. *Cell* **2020**, *181*, 271−280.e8.
(27) Wang, Q.; Zhang, Y.; Wu, L.; Niu, S.; Song, C.; Zhang, Z.; Lu, G.; Qiao, C.; Hu, Y.; Yuen, K.-Y.; Wang, Q.; Zhou, H.; Yan, J.; Qi, J. Structural and Functional Basis of SARS-CoV-2 Entry by Using Human ACE2. *Cell* **2020**, *181*, 894−904.e9.
(28) Roeters, S. J.; Iyer, A.; Pletikapić, G.; Kogan, V.; Subramaniam, V.; Woutersen, S. Evidence for Intramolecular Antiparallel Beta-Sheet Structure in Alpha-Synuclein Fibrils from a Combination of Two-Dimensional Infrared Spectroscopy and Atomic Force Microscopy. *Sci. Rep.* **2017**, *7*, 41051.
(29) Ulman, A.; Eilers, J. E.; Tillman, N. Packing and Molecular Orientation of Alkanethiol Monolayers on Gold Surfaces. *Langmuir* **1989**, *5*, 1147−1152.
(30) Weidner, T.; Shaporenko, A.; Müller, J.; Schmid, M.; Cyganik, P.; Terfort, A.; Zharnikov, M. Effect of the Bending Potential on Molecular Arrangement in Alkaneselenolate Self-Assembled Monolayers. *J. Phys. Chem. C* **2008**, *112*, 12495−12506.
(31) Alamdari, S.; Roeters, S. J.; Golbek, T. W.; Schmüser, L.; Weidner, T.; Pfaendtner, J. Orientation and Conformation of Proteins at the Air-Water Interface Determined from Integrative Molecular Dynamics Simulations and Sum Frequency Generation Spectroscopy. *Langmuir* **2020**, *36*, 11855−11865.
(32) Ulmschneider, M. B.; Sansom, M. S. P.; Di Nola, A. Evaluating Tilt Angles of Membrane-Associated Helices: Comparison of Computational and NMR Techniques. *Biophys. J.* **2006**, *90*, 1650−1660.
(33) Tan, J.; Zhang, J.; Luo, Y.; Ye, S. Misfolding of a Human Islet Amyloid Polypeptide at the Lipid Membrane Populates through β-Sheet Conformers without Involving α-Helical Intermediates. *J. Am. Chem. Soc.* **2019**, *141*, 1941−1948.
(34) Zhang, J.; Tan, J.; Pei, R.; Ye, S. Acidic Environment Significantly Alters Aggregation Pathway of Human Islet Amyloid Polypeptide at Negative Lipid Membrane. *Langmuir* **2020**, *36*, 1530−1537.
(35) Strazdaite, S.; Roeters, S. J.; Sakalauskas, A.; Sneideris, T.; Kirschner, J.; Pedersen, K. B.; Schiøtt, B.; Jensen, F.; Weidner, T.; Smirnovas, V.; Niaura, G. Interaction of Amyloid-β-(1-42) Peptide and Its Aggregates with Lipid/Water Interfaces Probed by Vibrational Sum-Frequency Generation Spectroscopy. *J. Phys. Chem. B* **2021**, *125*, 11208−11218.

https://doi.org/10.1021/acs.jpcb.2c01272
J. Phys. Chem. B XXXX, XXX, XXX−XXX